Climate Projections Very Likely Underestimate Future Volcanic Forcing and its Climatic Effects

Man Mei Chim[1], Thomas Jacques Aubry[2], Nathan Luke Abraham[3], Lauren Marshall[4], Jane Patricia Mulcahy[5], Jeremy Walton[5], and Anja Schmidt[1,6]

[1]University of Cambridge
[2]University of Exeter
[3]NCAS, University of Cambridge
[4]University of Durham
[5]Met Office Hadley Centre
[6]Institute of Atmospheric Physics (IPA), German Aerospace Center (DLR)

March 26, 2023

Abstract

Standard climate projections represent future volcanic eruptions by a constant forcing inferred from 1850-2014 volcanic forcing. Using the latest ice-core and satellite records to design stochastic eruption scenarios, we show that there is a 95% probability that explosive eruptions could emit more sulfur dioxide (SO_2) into the stratosphere over 2015-2100 than current standard climate projections (i.e., ScenarioMIP). Our simulations using the UK Earth System Model with interactive stratospheric aerosols show that for a median future eruption scenario, the 2015-2100 average global-mean stratospheric aerosol optical depth (SAOD) is double that used in ScenarioMIP, with small-magnitude eruptions ($<$ 3 Tg of SO_2) contributing 50% to SAOD perturbations. We show that volcanic effects on large-scale climate indicators, including global surface temperature, sea level and sea ice extent, are underestimated in ScenarioMIP because current climate projections do not fully account for the recurrent frequency of volcanic eruptions of different magnitudes.

Climate Projections Very Likely Underestimate Future Volcanic Forcing and its Climatic Effects

Man Mei Chim[1], Thomas J. Aubry[2], Nathan Luke Abraham[1,3], Lauren Marshall[4], Jane Mulcahy[5], Jeremy Walton[5], Anja Schmidt[1,6,7]

[1] Centre for Atmospheric Science, Yusuf Hamied Department of Chemistry, University of Cambridge, Cambridge, United Kingdom
[2] Department of Earth and Environmental Sciences, University of Exeter, Penryn, United Kingdom
[3] National Centre for Atmospheric Science, United Kingdom
[4] Department of Earth Sciences, Durham University, Durham, United Kingdom
[5] Met Office, FitzRoy Road, Exeter, United Kingdom
[6] German Aerospace Center (DLR), Institute of Atmospheric Physics (IPA), Oberpfaffenhofen, Germany
[7] Ludwig-Maximilians University Munich, Meteorological Institute, Munich, Germany

Corresponding author: Man Mei Chim (mmc70@cam.ac.uk)

Key Points:

- There is a 95% chance that the time-averaged 2015-2100 volcanic SO_2 flux from explosive eruptions exceeds the time-averaged 1850-2014 flux
- Standard climate projections very likely underestimate the 2015-2100 stratospheric aerosol optical depth and volcanic climate effects
- Small-magnitude eruptions (< 3 Tg SO_2) contribute 30% to 50% of the volcanic climate effects in a median future eruption scenario

Abstract

Standard climate projections represent future volcanic eruptions by a constant forcing inferred from 1850-2014 volcanic forcing. Using the latest ice-core and satellite records to design stochastic eruption scenarios, we show that there is a 95% probability that explosive eruptions could emit more sulfur dioxide (SO_2) into the stratosphere over 2015-2100 than current standard climate projections (i.e., ScenarioMIP). Our simulations using the UK Earth System Model with interactive stratospheric aerosols show that for a median future eruption scenario, the 2015-2100 average global-mean stratospheric aerosol optical depth (SAOD) is double that used in ScenarioMIP, with small-magnitude eruptions (< 3 Tg of SO_2) contributing 50% to SAOD perturbations. We show that volcanic effects on large-scale climate indicators, including global surface temperature, sea level and sea ice extent, are underestimated in ScenarioMIP because current climate projections do not fully account for the recurrent frequency of volcanic eruptions of different magnitudes.

Plain Language Summary

Climate projections are the simulations of Earth's climate in the future using complex climate models. Standard climate projections, as in Intergovernmental Panel on Climate Change Sixth Assessment Report, assume that explosive volcanic activity over 2015-2100 are of the same level as the 1850-2014 period. Using the latest ice-core and satellite records, we find that explosive eruptions could emit more sulfur dioxide into the upper atmosphere for the period of 2015-2100 than standard climate projections. Our climate model simulations show that the impacts of volcanic eruptions on climate, including global surface temperature, sea level and sea ice extent, are underestimated because current climate projections do not fully account for the recurrent frequency of volcanic eruptions. We also find that small-magnitude eruptions occur frequently and can contribute a significant effect on future climate.

1. Introduction

Large explosive volcanic eruptions can inject sulfur dioxide (SO_2) forming volcanic sulfate aerosols in the stratosphere that scatter incoming solar radiation, resulting in negative radiative forcing and global surface cooling for 1-3 years (McCormick et al., 1995). Stratospheric volcanic sulfate aerosols also heat the stratosphere by absorbing infrared and near-infrared radiation, which can further induce complex climate responses on seasonal to multi-decadal timescales (see Marshall et al. (2022) for a review).

As we cannot predict future volcanic eruptions, a constant volcanic forcing is commonly used in climate projections, e.g., as done in Phase 6 of the Coupled Model Intercomparison Project (CMIP6; Eyring et al., 2016), which informs the Intergovernmental Panel on Climate Change (IPCC) Sixth Assessment Report. In the CMIP6 Scenario MIP (ScenarioMIP; O'Neill et al., 2016), the constant volcanic forcing is inferred from the time average of the reconstructed 1850-2014 volcanic forcing. This approach does not account for how the sporadic occurrence of volcanic eruptions may affect the climate as opposed to a time-averaged forcing. In addition, volcanic injections into the stratosphere during the Holocene (past 11,500 years; Sigl et al., 2022) can vary by as much as a factor of 25 on centennial timescales. The corresponding uncertainty on future volcanic forcing is currently unaccounted for in most climate projections. A handful of studies have attempted to quantify the role of volcanic forcing uncertainty in climate projections (Ammann and Naveau, 2010; Bethke et al., 2017; Dogar et al., 2020). Bethke et al. (2017) estimated the volcanic forcing of 60 different future eruption scenarios from 2015 to 2100 by resampling ice-core sulfate deposition records going back 2,500 years (Sigl et al., 2015). Up-to-date ice-core and satellite volcanic sulfur emission datasets enable us to account for the occurrence of (i) eruptions larger in magnitude than those that occurred between 1850 and 2014, which injected as much as 300 Tg of SO_2 into the atmosphere, and (ii) small-magnitude eruptions below the detection threshold of ice-core datasets (Figure 1a), which can contribute a significant fraction to stratospheric aerosol optical depth (SAOD) (Santer et al., 2014; Schmidt et al., 2018).

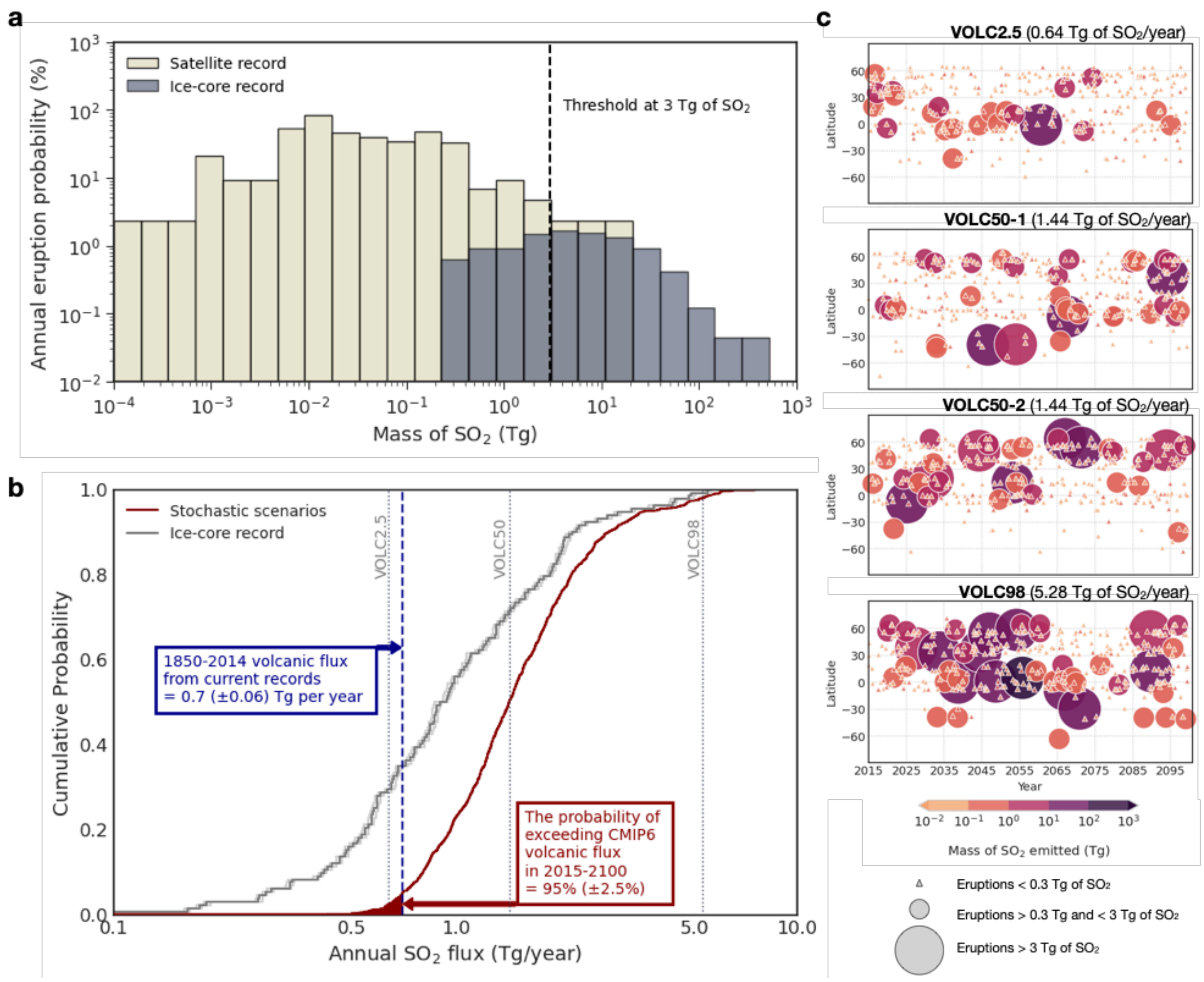

Figure 1. (**a**) Annual eruption probability based on ice-core (Sigl et al., 2022) and satellite (Carn et al., 2022) datasets. (**b**) Empirical cumulative probability density function of the SO_2 mass distribution of the 1000-member stochastic scenarios and the Holvol ice-core dataset (with 95% bootstrap confidence bounds, in light grey). We estimate the probability of exceeding CMIP6 volcanic flux using the 1850-2014 flux from current volcanic SO_2 emission records (Neely and Schmidt, 2016; Sigl et al., 2022; Carn, 2022). (**c**) Eruption time series of VOLC2.5, VOLC50-1, VOLC50-2, and VOLC98 with annual volcanic SO_2 flux of each scenario in brackets.

In addition, whether they apply a constant volcanic forcing (e.g., CMIP6 ScenarioMIP) or use stochastic eruption scenarios (Bethke et al., 2017), existing climate projections use prescribed volcanic aerosol optical properties derived from simplified volcanic aerosol models. Climate models with interactive stratospheric aerosols (Timmreck et al., 2018) showed a better agreement between the simulated surface temperature responses and tree-ring surface temperature reconstructions for the 1257 Mount Samalas and 1815 Mount Tambora eruptions (Stoffel et al., 2015) and the 1783-1784 Laki eruption (Pausata et al., 2015; Zambri et al., 2019). Furthermore, the prescribed aerosol approach cannot account for the impacts of global warming on the life cycle of volcanic sulfate aerosols (Aubry et al., 2021), including the impact of changing atmospheric stratification on volcanic plume height (Aubry et al., 2019). Such climate-volcano feedbacks might amplify the peak global-mean radiative forcing associated with large-magnitude tropical eruptions by 30% (Aubry et al., 2021).

Our study aims to improve our understanding of future volcanic impacts on climate. To this end, we perform model simulations from 2015 to 2100 with two innovations: (i) a stochastic resampling approach using the latest ice-core and satellite datasets to generate improved future volcanic eruption scenarios; and (ii) a plume-aerosol-chemistry-climate modeling framework (named UKESM-VPLUME), which combines a volcanic plume model and an Earth System Model with interactive stratospheric aerosols to simulate volcanic climate effects while accounting for climatic controls on plume-rise height.

2. Methodology

2.1 Stochastic future eruption scenarios

We generate 1000 stochastic future eruption scenarios for 2015 to 2100 by resampling SO_2 mass from volcanic emission inventories from a bipolar ice-core array covering the past 11,500 years (Holvol; Sigl et al., 2022) and a multi-satellite record from 1979 to 2021 (Carn et al., 2016; Carn, 2022) (Figure 1a and S1). Before resampling, we filter out: i) effusive eruptions; ii) in the satellite record, eruptions with eruptive plume heights more than 3 km below the thermal tropopause (obtained from NCEP/NCAR Reanalysis 1; Kalnay et al., 1996); we assume that aerosol lofting could result in stratospheric injections for tropospheric plumes less than 3 km below the tropopause. By examining the eruption frequency-magnitude (i.e., in this study, SO_2 mass) distribution of both ice-core and satellite records (Figure 1a), we identify 3 Tg of SO_2 as a threshold: i) below which ice-core records underestimate eruption frequency due to under-recording; and ii) above which the short duration of the satellite record precludes it from capturing the true frequency of eruptions with higher magnitude. Accordingly, we use a 3 Tg of SO_2 threshold to define "small-magnitude" and "large-magnitude" eruptions. We resample small-magnitude eruptions from the satellite record only, and large-magnitude ones from the combined ice-core and satellite record. Details of the resampling of the erupting volcano, SO_2 mass, and mass eruption rate are discussed in the Supplementary Information.

2.2 UKESM-VPLUME

Atmospheric stratification, wind and humidity affect volcanic plume dynamics and SO_2 injection height (e.g., Mastin, 2014), but SO_2 height is commonly prescribed in modelling studies of volcanic forcing (e.g., Timmreck et al., 2018). To account for meteorological controls on plume dynamics, we have developed UKESM-VPLUME, which couples the UK Earth System Model (UKESM; Mulcahy et al., 2023) with Plumeria (1-D eruptive plume model; Mastin, 2007, 2014) (details in Supplementary Information). We use version 1.1 of UKESM with fully-coupled atmosphere-land-ocean and interactive stratospheric aerosols. In brief, for each time step of the UKESM atmospheric model during an eruption, UKESM-VPLUME interactively passes the atmospheric conditions simulated at the eruption location to Plumeria. Plumeria then computes the neutral buoyancy height of the volcanic plume based on atmospheric conditions and the mass eruption rate generated for each eruption in the stochastic scenarios. Volcanic SO_2 is injected into UKESM at the neutral buoyancy height calculated in Plumeria using a gaussian profile with a width of 10% of the plume height (consistent with large-eddy simulations of volcanic plumes, Aubry et al., 2019). This approach ensures that plume heights of volcanic eruptions are consistent with the meteorological conditions simulated by UKESM.

2.3 Experimental design

We perform simulations using the UKESM-VPLUME framework for four stochastic future eruption scenarios at the 2.5th, 50.0th, 50.5th and 98.0th percentiles (termed VOLC2.5, VOLC50-1, VOLC50-2, VOLC98) of the distribution of the 2015-2100 average SO_2 flux across the 1000 future eruption scenarios (Figure 1b). We choose scenarios close (within 0.5 percentile) to the 2.5th, 50th and 97.5th to sample the median and 95% confidence interval of the future volcanic stratospheric SO_2 injections. To test future climate trajectory sensitivity to the temporal and spatial distribution of eruptions, we run two scenarios near the 50th percentile. For instance, VOLC50-2 has more large-magnitude eruptions than VOLC50-1 in the early 21st century (Figure 1c). We also performed the VOLC50 runs with small-magnitude eruptions only (VOLC50-1S and VOLC50-2S) to isolate their contribution to the overall climate effects caused by eruptions of all magnitudes. We compare the results from VOLC runs with runs without volcanic eruptions (NOVOLC) and with CMIP6 ScenarioMIP constant volcanic forcing (CONST). We perform all simulations from 2015 to 2100 under a high-end future emission scenario (SSP3-7.0 in ScenarioMIP) running three ensemble members for each scenario.

3. Results

Figure 2 shows the global monthly-mean SAOD at 550 nm and the time-averaged values over 2015-2100. The time-averaged ensemble-mean SAOD ranges from 0.015 ± 0.0004 (VOLC2.5) to 0.062 ± 0.0018 (VOLC98), with an average value of 0.024 ± 0.0012 for the two median future eruption scenarios (VOLC50), while the SAOD in CONST, which followed the ScenarioMIP design, is 0.012 ± 0.0018 (one standard deviation uncertainty). Small-magnitude eruptions contribute 0.010 to 0.013 ± 0.0002 to the time-averaged SAOD in the VOLC50 scenarios, i.e., about 50% of the total SAOD. Comparing VOLC2.5 to CONST and assuming that the rank for the 2015-2100-year mean volcanic SO_2 flux and SAOD are the same, it is thus very likely (i.e., > 90% probability following IPCC guidance note; Mastrandrea et al., 2010) that the actual global 2015-2100 mean SAOD will be higher than that prescribed in ScenarioMIP, with the median (VOLC50) SAOD value being double that used in ScenarioMIP. The result is consistent with Figure 1, given that the 1850-2014 time-averaged SO_2 flux used to define the ScenarioMIP volcanic forcing is close to the 2.5th percentile of the future volcanic SO_2 flux distribution. Beyond the time-averaged SAOD value, owing to the sporadic nature of volcanic eruptions, the global monthly-mean SAOD values in VOLC scenarios can be up to a factor of 60 greater than that in ScenarioMIP (Figures 2 and S2).

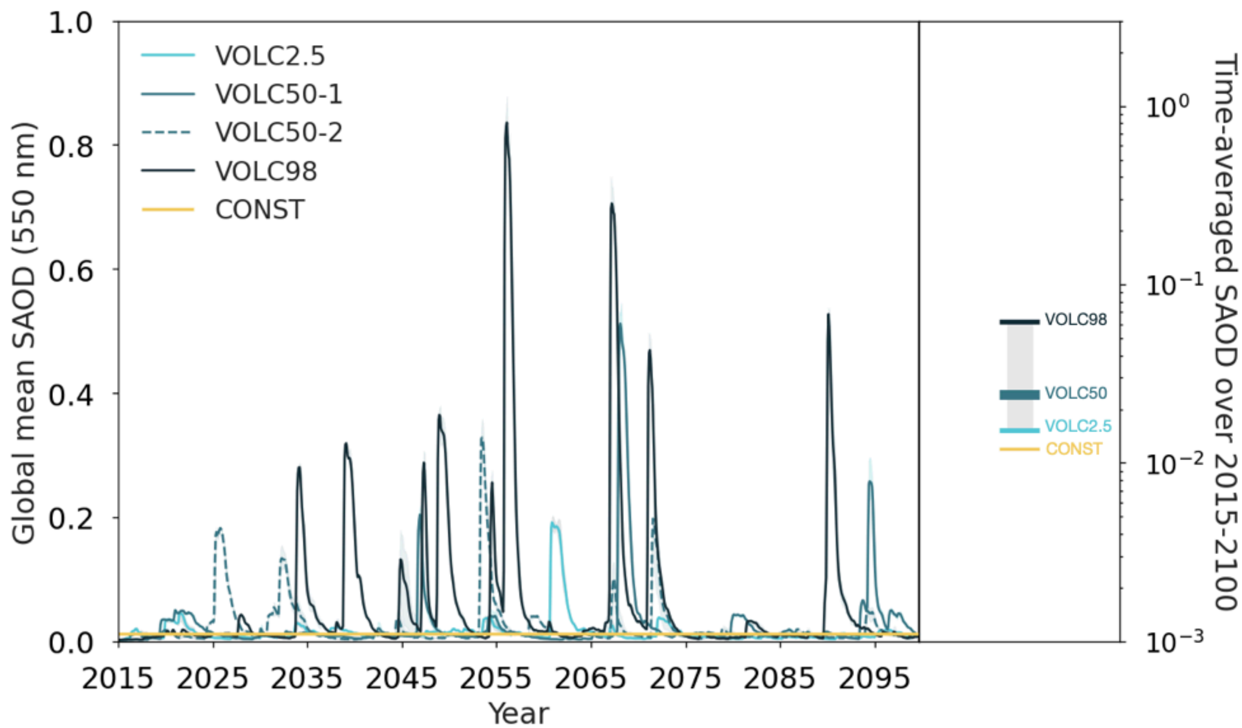

Figure 2. (Left) Global monthly-mean SAOD at 550 nm. The lines show the ensemble mean and the shading shows the spread of the maximum and minimum ensemble members. (Right) The corresponding time-averaged SAOD over 2015-2100 (in log scale).

Figure 3a shows the global annual-mean surface air temperature at 1.5 m (GMST) relative to the 1850-1900 period. Large-magnitude volcanic eruptions lead to a short-term drop in the annual-mean GMST for at least 1 year and up to 6 to 7 years for the largest eruptions. In the VOLC98 scenario where clusters of large-magnitude eruptions occur, they can induce multi-decadal global cooling. The 2015-2100 time-averaged GMST relative to detrended NOVOLC ensemble mean (Figure 3b) ranges between -0.16 ºC (VOLC2.5) and -0.56 ºC (VOLC98), with CONST lying outside this range at -0.12 ºC. Volcanic cooling for median eruption scenarios (VOLC50-1 and VOLC50-2) is 0.20 to 0.24 ºC, double that of CONST, and 0.09 to 0.10 ºC of cooling is attributable to small-magnitude eruptions (Table S1).

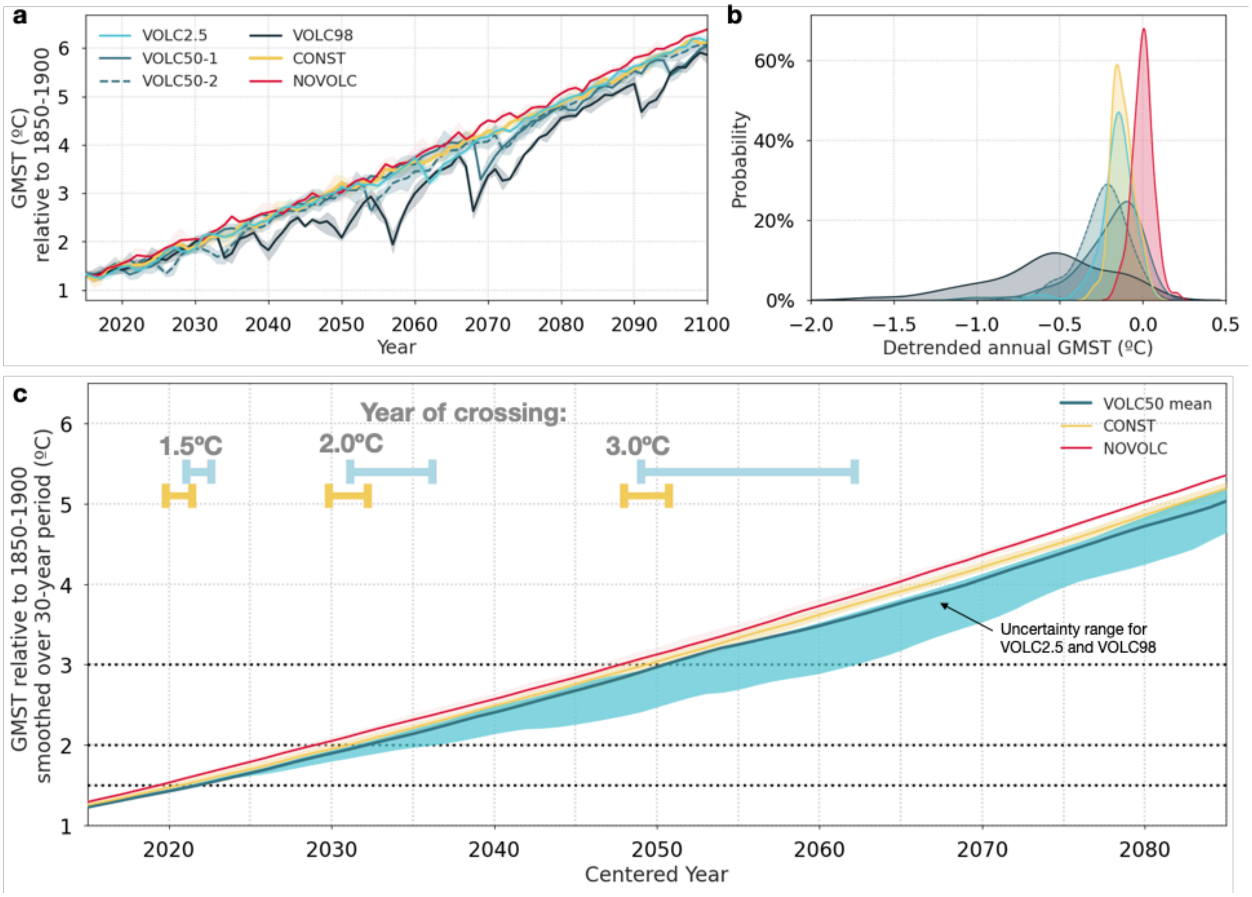

Figure 3. (**a**) Annual-mean GMST relative to 1850-1900. The lines show the ensemble mean and the shading shows the spread of the maximum and minimum ensemble members. (**b**) Probability density function of the annual-mean GMST relative to detrended NOVOLC ensemble mean (see Supplementary Information). (**c**) 30-year moving mean GMST with years of crossing 1.5 ºC, 2 ºC, and 3 ºC for VOLC and CONST runs.

The IPCC defines global warming as an increase, relative to 1850-1900, in the global mean surface air and sea surface temperatures over a period of 30 years (IPCC, 2021). Using this definition, we examine the year of crossing of 1.5 ºC, 2 ºC, and 3 ºC warming thresholds for VOLC and CONST runs (Figure 3c). Volcanic eruptions delay the time of crossing 1.5 ºC by about 1.6 to 3.2 years when compared to NOVOLC (Table S2), consistent with Bethke et al. (2017). Compared to CONST, times of temperature threshold crossings are significantly delayed by 1.8 to 2.5 years in VOLC50-2, but unaffected in VOLC50-1. This highlights the sensitivity of the time of crossing to the temporal distribution of large-magnitude eruptions. The occurrence of volcanic clusters in VOLC98 causes an extended cooling period between 2034 to 2060 (Figure 3a) which delays the crossing of 2 ºC and 3 ºC by 7 and 14 years, respectively.

In Figure 4, we examine volcanic effects on large-scale climate indicators other than GMST. The 2015-2100 time-averaged global annual-mean precipitation fluxes in all VOLC runs show a greater reduction than CONST, with a range between -0.014 mm/day (VOLC2.5) to -0.052 mm/day (VOLC98), and -0.010 mm/day for CONST (Figure 4a). In VOLC50 scenarios, the global annual-mean precipitation flux is reduced by 0.019 mm/day with small-magnitude eruptions alone contributing between 0.008 and 0.009 mm/day, comparable to the effects of the volcanic forcing implemented in ScenarioMIP. It is thus very likely that the reduction of global mean precipitation due to volcanic effects is underestimated in ScenarioMIP.

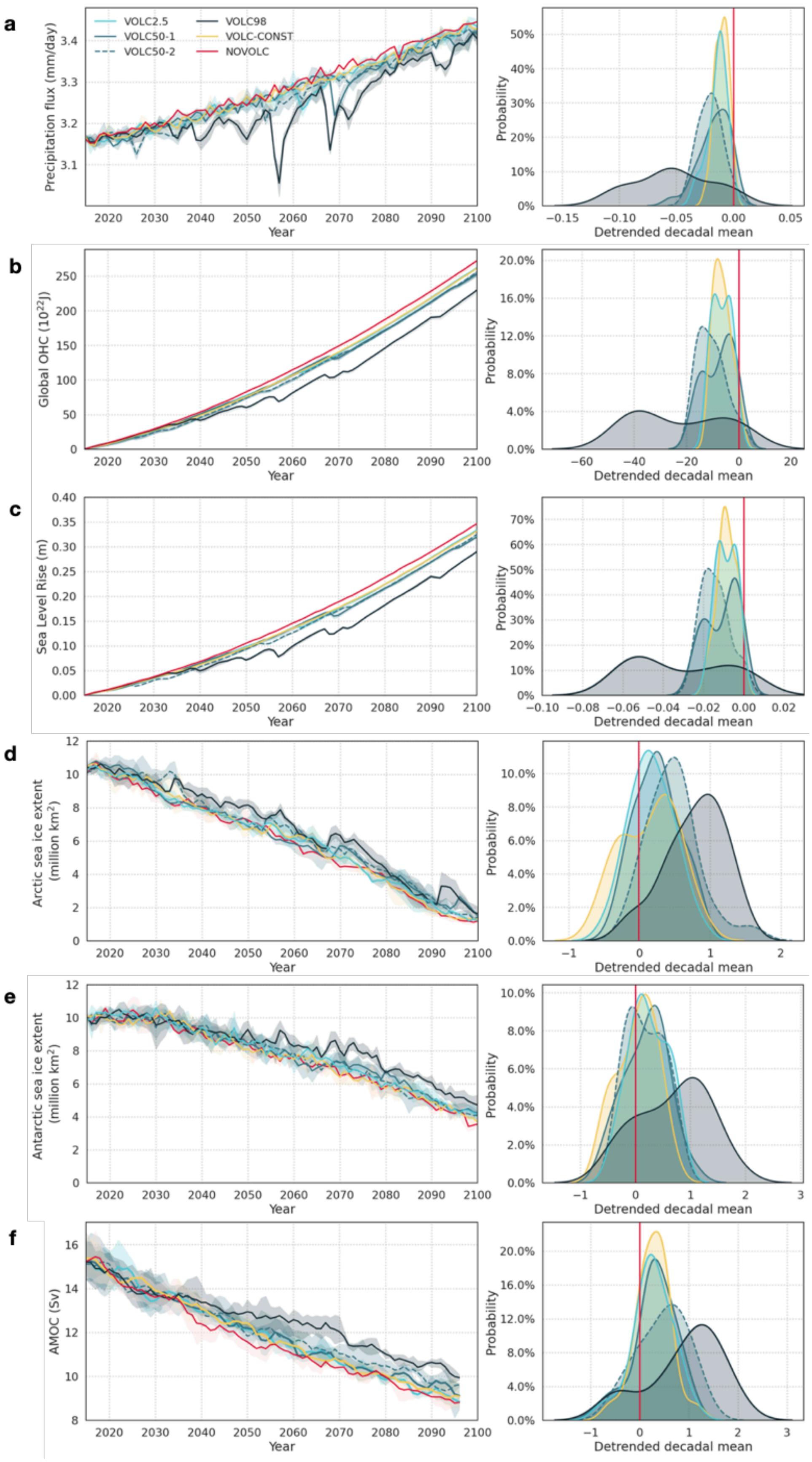

a
VOLC2.5
VOLC50-1
VOLC50-2
VOLC98
VOLC-CONST
NOVOLC
Precipitation flux (mm/day)
Probability
Year
Detrended decadal mean
b
Global OHC (10^{22}J)
Probability
Year
Detrended decadal mean
c
Sea Level Rise (m)
Probability
Year
Detrended decadal mean
d
Arctic sea ice extent (million km^2)
Probability
Year
Detrended decadal mean
e
Antarctic sea ice extent (million km^2)
Probability
Year
Detrended decadal mean
f
AMOC (Sv)
Probability
Year
Detrended decadal mean

Figure 4. (Left) Annual mean time series of selected large-scale climate indicators. The line shows the ensemble mean and the shading shows the spread of the maximum and minimum ensemble members. (Right) The corresponding decadal-mean probability density function relative to the detrended NOVOLC ensemble mean, with the red vertical line showing the mean of NOVOLC. (**a**) global precipitation flux (in mm/day), (**b**) global ocean heat content (in 10^{22} J), (**c**) global thermosteric sea level rise (in m), (**d** and **e**) Arctic and Antarctic sea ice extent (in million km^2), defined as the area with >15% sea ice, (f) 5-year moving mean AMOC at 26ºN (in Sv).

Volcanic-induced surface cooling penetrates into the deep ocean layer and decreases the global ocean heat content (Figures 4b and S3), which in turn leads to less thermal expansion in seawater and a reduction in thermosteric sea level (Figure 4c). Volcanic forcing in VOLC50 reduces global ocean heat content and thermosteric sea level by 6% to 7% compared to NOVOLC by 2100, whereby about half is attributed to small-magnitude eruptions (Figure S3). Although volcanic forcing can cause considerable impacts on large-scale ocean metrics, it does not offset the anthropogenic-induced ocean warming trends even for the upper-end volcanic emission scenario VOLC98 (Figures 4b, 4c and 4f).

Depending on the eruption magnitude and location, the Arctic and Antarctic sea ice extents show an immediate increase for 1-2 years after large-magnitude eruptions (Figures 4d and 4e). The time-averaged global sea ice extent in VOLC runs over 2015 to 2100 increases by 0.43 million km^2 (VOLC2.5) to 1.53 million km^2 (VOLC98) as compared to 0.20 million km^2 for CONST. Comparing VOLC2.5 to CONST suggests that for similar time-averaged SAOD, the use of a constant forcing instead of a stochastic eruption distribution halves the magnitude of the sea ice response.

The time-averaged Atlantic Meridional Overturning Circulation (AMOC) at 26ºN over 2015 to 2100 is strengthened by between 0.26 Sv (VOLC2.5) and 0.93 Sv (VOLC98) as compared to NOVOLC, with all VOLC scenarios exhibiting an increased decadal mean AMOC strength (Figure 4f). The stronger AMOC responses in VOLC runs are consistent with reduced precipitation over the Northern Hemisphere, which increases salinity and enhances deep-water formation (Pausata et al., 2015). Small-magnitude eruptions alone can increase the time-averaged AMOC strength by 0.36-0.38 Sv (VOLC50-1S and VOLC50-2S), which is greater than CONST at 0.28 Sv, and contribute to over 77% of the AMOC response in the median future scenarios (Table S1). One of the median future scenarios (VOLC50-1) has a weaker time-averaged AMOC than the same run with small-magnitude eruptions only (VOLC50-1S) due to an extended period of weakened AMOC after the occurrence of large-magnitude eruptions (Figure S4), suggesting AMOC may have different responses towards different latitudinal and SO_2 distributions of large-magnitude eruptions.

4. Discussion

Small-magnitude eruptions (< 3 Tg of SO_2) contribute a considerable fraction (between 33% and 40%) of the total upper atmospheric volcanic SO_2 emissions in VOLC50, and in turn, are responsible for 30% to 50% of the volcanic impact on selected large-scale climate indicators and over 77% of the AMOC response (Figure 5 and Table S1). For future eruption scenarios with fewer eruptions than VOLC50, the contribution from small-magnitude eruptions is expected to be even greater because the total mass injected by small-magnitude eruptions is relatively similar across all scenarios. Despite the importance of volcanic forcing from small-magnitude eruptions, they are mostly unaccounted for in historical simulations before satellite measurements are available. In the pre-satellite historical period (1850-1978), the Neely and Schmidt (2016) and Sigl et al. (2022) volcanic SO_2 inventories have an average flux of 0.21 and 0.26 Tg of SO_2 per year from small-magnitude eruptions, respectively. By comparison, the flux is 0.50 Tg of SO_2 per year over 1979-2021 (Carn, 2022). This suggests a missing flux from small-magnitude eruptions of between 0.24 and 0.29 Tg of SO_2 per year in the pre-satellite historical period, which is the equivalent of injections from about 1 to 2 Mount Pinatubo 1991 eruptions.

Our stochastic scenarios imply that CMIP6 ScenarioMIP very likely (95 ± 2.5%) underestimates the 2015-2100 volcanic SO_2 flux from explosive eruptions and, in turn, forcing (Figure 1b). Figure 1b shows the cumulative probability against the annual SO_2 flux obtained by resampling ice-core record of volcanic SO_2 injection only (i.e., Holvol; Sigl et al. 2022) and both ice-core and satellite (Carn, 2022) records as in our stochastic scenarios. CMIP6 ScenarioMIP uses a constant volcanic forcing inferred from the 1850-2014 period during which the mean volcanic SO_2 flux recorded in emission inventories was 0.7 ± 0.06 Tg per year. However, we find a 95% confidence interval for the 2015-2100 mean volcanic SO_2 flux between 0.64 to 5.28 Tg per year in our eruption scenarios (Figure 1b). Our stochastic approach, which represents better the frequency-magnitude distribution of small-magnitude eruptions, results in a higher annual SO_2 flux than resampling from the ice-core record only (e.g., Bethke et al., 2017).

Our future volcanic eruption scenarios greatly enhance the variability of large-scale climate indicators as compared to the ScenarioMIP forcing (Figure 5). Future volcanic emissions in our scenarios cause a 3.5% (VOLC2.5) to 15.0% (VOLC98) decrease in the 2015-2100 time-averaged global net radiative forcing at the top-of-the-atmosphere relative to the anthropogenic contribution (Figures 5 and S5, see Supplementary Information). The time-averaged climate responses of our selected climate indicators scale with the magnitude of volcanic forcing except for the Antarctic sea ice extent and AMOC, which may depend on the latitudinal distribution of eruptions. We also find that the magnitude of volcanic effects on climate indicators are comparable between CONST and VOLC2.5, which is a scenario with only one Pinatubo-like eruption over 2015-2100. Our results suggest that due to the low volcanic forcing used in ScenarioMIP, it is very likely (97.5%) that ScenarioMIP underestimates the climate effects of the large-scale climate indicators examined in this study.

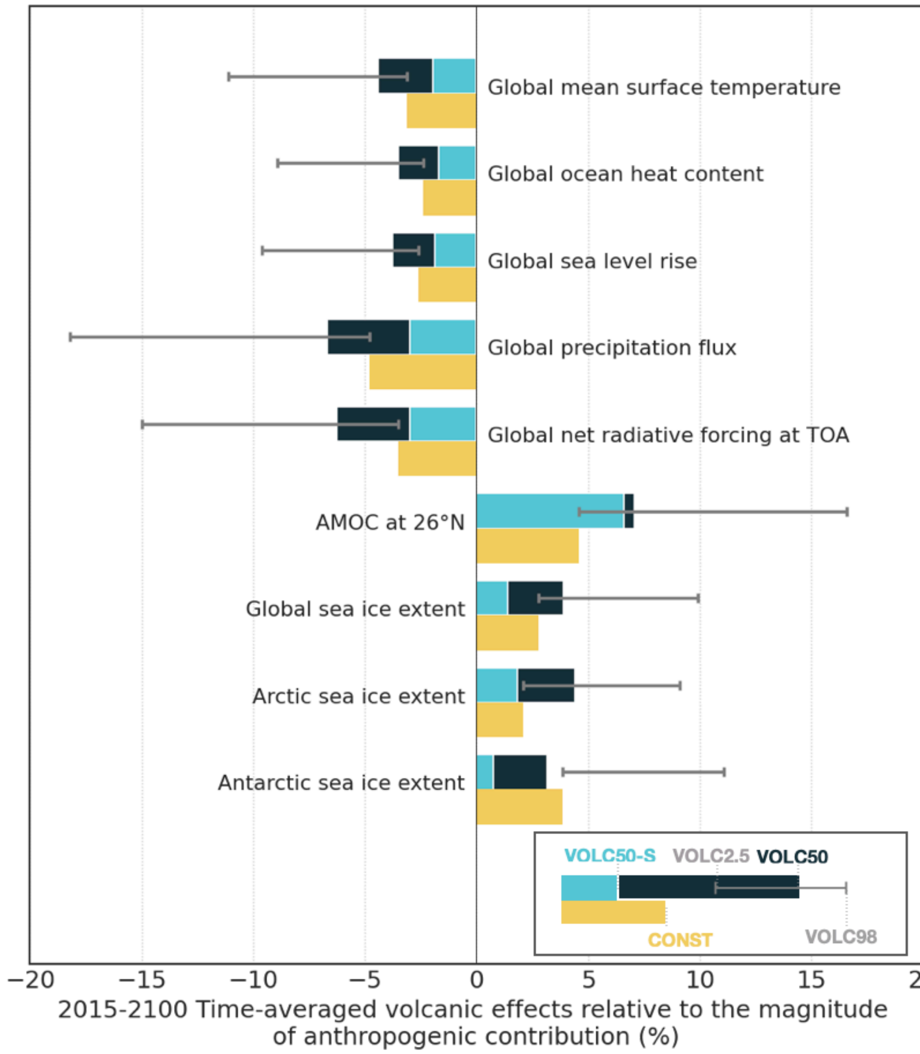

Figure 5. Bar chart showing the time-averaged volcanic effects on large-scale climate indicators relative to the magnitude of anthropogenic contribution over the period of 2015 to 2100, i.e., VOLC50-S refers to average effects of the two VOLC50 runs with small-magnitude eruptions only.

Our simulation results show that for the SSP3-7.0 scenario, volcanic forcing can offset 2.1% to 18.2% of the anthropogenic effects to large-scale climate indicators depending on the future eruption scenarios (Figure 5). In a future scenario with low-end anthropogenic emission (SSP1-2.6), we would expect the relative effect between future volcanism and anthropogenic forcing to be much greater, e.g., by a factor of 3 for GMST since the 2015-2100 warming is 4.8 ºC in SSP3-7.0 and 1.4 ºC in SSP1-2.6. Our work highlights how the high level of uncertainty on volcanic forcing affects climate projections. For the same future eruption scenario, the volcanic effects on climate will also vary between SSP scenarios owing to climate-volcano feedbacks (e.g., Hopcroft et al., 2017; Fasullo et al., 2018; Aubry et al., 2022), which need to be quantified.

5. Conclusion

We performed climate model simulations from 2015 to 2100 with stochastic future eruption scenarios using UKESM-VPLUME (a plume-aerosol-chemistry-climate model framework that accounts for climate-volcano feedbacks) to examine how the uncertainties on volcanic forcing affect climate projections. Using the latest ice-core and satellite datasets, we show that the 2015 to 2100 volcanic SO_2 flux from explosive eruptions has a 95% probability to exceed the 1850-2014 flux, which was used to derive volcanic forcing in CMIP6 ScenarioMIP. Our simulations suggest that the time-averaged SAOD in a median future scenario is 0.024 (95% uncertainty: 0.015-0.062), which is double that in ScenarioMIP, and that ScenarioMIP very likely underestimates the future volcanic effects on climate. Our study emphasizes the importance of the climate effects of future volcanic eruptions relative to the anthropogenic contribution, which even for an upper end anthropogenic forcing scenario (SSP3-7.0) can range between 2.1% to 18.2% for large-scale climate indicators. We also highlight the climate-relevance of small-magnitude eruptions, which are responsible for 30% to 50% of the volcanic effects on selected climate indicators. Future climate projection studies could either use our stochastic eruption scenarios generated using state-of-the-art volcanic emission inventories, or use a time-averaged constant forcing that better represents long-term volcanic activity and accounts for small-magnitude eruption contributions.

Acknowledgements

The authors declare no conflict of interests. We sincerely thank Robin Smith and Till Kuhlbrodt for their suggestions in the analysis, and Larry Mastin who provided the latest version of Plumeria model for developing UKESM-VPLUME framework. M.M. Chim is supported by the Croucher Foundation and The Cambridge Commonwealth, European & International Trust through a Croucher Cambridge International Scholarship. Jane Mulcahy and Jeremy Walton were supported Met Office Hadley Centre Climate Programme, funded by BEIS.

Data Availability Statement

The data presented in this study are available in the University of Cambridge data repository: https://doi.org/10.17863/CAM.94912. All data used for this study is with the license Creative Commons Attribution 4.0 International (CC-BY-4.0).

References

Ammann, C. M., & Naveau, P. (2010). A statistical volcanic forcing scenario generator for climate simulations. *Journal of Geophysical Research: Atmospheres*, *115*(D5). https://doi.org/10.1029/2009JD012550

Archibald, A. T., O'Connor, F. M., Abraham, N. L., Archer-Nicholls, S., Chipperfield, M. P., Dalvi, M., Folberth, G. A., Dennison, F., Dhomse, S. S., Griffiths, P. T., Hardacre, C., Hewitt, A. J., Hill, R. S., Johnson, C. E., Keeble, J., Köhler, M. O., Morgenstern, O., Mulcahy, J. P., Ordóñez, C., … Zeng, G. (2020). Description and evaluation of the UKCA stratosphere–troposphere chemistry scheme (StratTrop vn 1.0) implemented in UKESM1. *Geoscientific Model Development*, *13*(3), 1223–1266. https://doi.org/10.5194/gmd-13-1223-2020

Aubry, T. J., & Jellinek, A. M. (2018). New insights on entrainment and condensation in volcanic plumes: Constraints from independent observations of explosive eruptions and implications for assessing their impacts. *Earth and Planetary Science Letters*, 490, 132-142. https://doi.org/10.1016/j.epsl.2018.03.028

Aubry, T. J., Cerminara, M., & Jellinek, A. M. (2019). Impacts of Climate Change on Volcanic Stratospheric Injections: Comparison of 1-D and 3-D Plume Model Projections. *Geophysical Research Letters*, *46*(17–18), 10609–10618. https://doi.org/10.1029/2019GL083975

Aubry, T. J., Staunton-Sykes, J., Marshall, L. R., Haywood, J., Abraham, N. L., & Schmidt, A. (2021). Climate change modulates the stratospheric volcanic sulfate aerosol lifecycle and radiative forcing from tropical eruptions. *Nature Communications*, *12*(1), 4708. https://doi.org/10.1038/s41467-021-24943-7

Aubry, T. J., Farquharson, J. I., Rowell, C. R., Watt, S. F., Pinel, V., Beckett, F., Fasullo, J., Hopcroft, P. O., Pyle, D. M., Schmidt, A., & Sykes, J. S. (2022). Impact of climate change on volcanic processes: current understanding and future challenges. *Bulletin of Volcanology*, *84*(6), 1–11. https://doi.org/10.1007/s00445-022-01562-8

Bethke, I., Outten, S., Otterå, O. H., Hawkins, E., Wagner, S., Sigl, M., & Thorne, P. (2017). Potential volcanic impacts on future climate variability. *Nature Climate Change*, *7*(11), 799–805. https://doi.org/10.1038/nclimate3394

Butchart, N. (2014). The Brewer-Dobson circulation. Reviews of geophysics, 52 (2), 157–184. https://doi.org/10.1002/2013RG000448

Carn, S. A., Clarisse, L., & Prata, A. J. (2016). Multi-decadal satellite measurements of global volcanic degassing. *Journal of Volcanology and Geothermal Research*, *311*, 99–134. https://doi.org/10.1016/j.jvolgeores.2016.01.002

Carn, S. (2022). *Multi-Satellite Volcanic Sulfur Dioxide L4 Long-Term Global Database V4 (MSVOLSO2L4 4)* [Data set]. Goddard Earth Science Data and Information Services Center (GES DISC). https://disc.gsfc.nasa.gov/datasets/MSVOLSO2L4_4/summary

Costa, A., Suzuki, Y. J., Cerminara, M., Devenish, B. J., Ongaro, T. E., Herzog, M., Van Eaton, A. R., Denby, L., Bursik, M., Vitturi, M. d., et al. (2016). Results of the eruptive column model inter-comparison study. *Journal of Volcanology and Geothermal Research*, *326*, 2–25. https://doi.org/10.1016/j.jvolgeores.2016.01.017

Devenish, B., & Cerminara, M. (2018). The transition from eruption column to umbrella cloud. *Journal of Geophysical Research: Solid Earth*, *123*(12), 10–418. https://doi.org/10.1029/2018JB015841

Dhomse, S. S., Emmerson, K. M., Mann, G. W., Bellouin, N., Carslaw, K. S., Chipperfield, M. P., Hommel, R., Abraham, N. L., Telford, P., Braesicke, P., Dalvi, M., Johnson, C. E., O'Connor, F., Morgenstern, O., Pyle, J. A., Deshler, T., Zawodny, J. M., & Thomason, L. W. (2014). Aerosol microphysics simulations of the Mt. Pinatubo eruption with the UM-UKCA composition-climate model. *Atmospheric Chemistry and Physics*, *14*(20), 11221–11246. https://doi.org/10.5194/acp-14-11221-2014

Dogar, M. M., Sato, T., & Liu, F. (2020). Ocean Sensitivity to Periodic and Constant Volcanism. *Scientific Reports*, *10*(1), 293. https://doi.org/10.1038/s41598-019-57027-0

Eyring, V., Bony, S., Meehl, G. A., Senior, C. A., Stevens, B., Stouffer, R. J., & Taylor, K. E. (2016). Overview of the Coupled Model Intercomparison Project Phase 6 (CMIP6) experimental design and organization. *Geoscientific Model Development*, *9*(5), 1937–1958. https://doi.org/10.5194/gmd-9-1937-2016

Fasullo, J. T., Tilmes, S., Richter, J. H., Kravitz, B., MacMartin, D. G., Mills, M. J., & Simpson, I. R. (2018). Persistent polar ocean warming in a strategically geoengineered climate. *Nature Geoscience*, *11*(12), 910–914. https://doi.org/10.1038/s41561-018-0249-7

Fero, J., Carey, S. N., & Merrill, J. T. (2009). Simulating the dispersal of tephra from the 1991 Pinatubo eruption: Implications for the formation of widespread ash layers. *Journal of Volcanology and Geothermal Research*, *186*(1-2), 120-131. https://doi.org/10.1016/j.jvolgeores.2009.03.011

Gautier, E., Savarino, J., Hoek, J., Erbland, J., Caillon, N., Hattori, S., Yoshida, N., Albalat, E., Albarede, F., & Farquhar, J. (2019). 2600-years of stratospheric volcanism through sulfate isotopes. *Nature Communications*, *10*(1), 466. https://doi.org/10.1038/s41467-019-08357-0

Global Volcanism Program (2022). Volcanoes of the World (v. 4.11.1; 29 Aug 2022). [Database]. Distributed by Smithsonian Institution, compiled by Venzke, E. https://doi.org/10.5479/si.GVP.VOTW5-2022.5.0

Guo, S., Bluth, G. J., Rose, W. I., Watson, I. M., & Prata, A. J. (2004). Re-evaluation of SO2 release of the 15 June 1991 Pinatubo eruption using ultraviolet and infrared satellite sensors. *Geochemistry, Geophysics, Geosystems*, 5(4). https://doi.org/10.1029/2003GC000654

Hersbach, H., Bell, B., Berrisford, P., Biavati, G., Horányi, A., Muñoz Sabater, J., Nicolas, J., Peubey, C., Radu, R., Rozum, I., Schepers, D., Simmons, A., Soci, C., Dee, D., Thépaut, J-N. (2019). *ERA5 monthly averaged data on pressure levels from 1979 to present* [Data set]. Copernicus Climate Change Service (C3S) Climate Data Store (CDS). doi: 10.24381/cds.6860a573

Hopcroft, P. O., Kandlbauer, J., Valdes, P. J., & Sparks, R. S. J. (2018). Reduced cooling following future volcanic eruptions. *Climate Dynamics*, *51*(4), 1449–1463. https://doi.org/10.1007/s00382-017-3964-7

IPCC, 2021: Climate Change 2021: The Physical Science Basis. Contribution of Working Group I to the Sixth Assessment Report of the Intergovernmental Panel on Climate Change [Masson-Delmotte, V., P. Zhai, A. Pirani, S.L. Connors, C. Péan, S. Berger, N. Caud, Y. Chen, L. Goldfarb, M.I. Gomis, M. Huang, K. Leitzell, E. Lonnoy, J.B.R. Matthews, T.K. Maycock, T. Waterfield, O. Yelekçi, R. Yu, and B. Zhou (eds.)]. Cambridge University Press, Cambridge, United Kingdom and New York, NY, USA, In press, doi:10.1017/9781009157896.

Kalnay, E., Kanamitsu, M., Kistler, R., Collins, W., Deaven, D., Gandin, L., Iredell, M., Saha, S., White, G., Woollen, J., Zhu, Y., Chelliah, M., Ebisuzaki, W., Higgins, W., Janowiak, J., Mo, K. C., Ropelewski, C., Wang, J., Leetmaa, A., Reynolds, R., Jenne, R., & Joseph, D. (1996). The NCEP/NCAR 40-Year Reanalysis Project, *Bulletin of the American Meteorological Society*, *77*(3), 437–472. https://doi.org/10.1175/1520-0477(1996)077<0437:TNYRP>2.0.CO;2

Marshall, L. R., Maters, E. C., Schmidt, A., Timmreck, C., Robock, A., & Toohey, M. (2022). Volcanic effects on climate: recent advances and future avenues. *Bulletin of Volcanology*, *84*(5), 1–14. https://doi.org/10.1007/s00445-022-01559-3

Mastin, L. G. (2007). A user-friendly one-dimensional model for wet volcanic plumes. *Geochemistry, Geophysics, Geosystems*, *8*(3). https://doi.org/10.1029/2006GC001455

Mastin, L. G. (2014). Testing the accuracy of a 1-D volcanic plume model in estimating mass eruption rate. *Journal of Geophysical Research: Atmospheres*, *119*(5), 2474–2495. https://doi.org/10.1002/2013JD020604

Mastrandrea, M. D., Field, C. B., Stocker, T. F., Edenhofer, O., Ebi, K. L., Frame, D. J., Held, H., Kriegler, E., Mach, K. J., Matschoss, P. R., Plattner, G. K. (2010). Guidance note for lead authors of the IPCC fifth assessment report on consistent treatment of uncertainties. https://

www.ipcc.ch/site/assets/uploads/2017/08/AR5_Uncertainty_Guidance_Note.pdf

McCormick, M. P., Thomason, L. W., & Trepte, C. R. (1995). Atmospheric effects of the Mt Pinatubo eruption. *Nature*, *373*(6513), 399–404. https://doi.org/10.1038/373399a0

Neely III, R.R. & Schmidt, A. (2016). *VolcanEESM: Global volcanic sulphur dioxide (SO2) emissions database from 1850 to present - Version 1.0* [Data set]. Centre for Environmental Data Analysis. http://dx.doi.org/10.5285/76ebdc0b-0eed-4f70-b89e-55e606bcd568

O'Neill, B. C., Tebaldi, C., van Vuuren, D. P., Eyring, V., Friedlingstein, P., Hurtt, G., Knutti, R., Kriegler, E., Lamarque, J.-F., Lowe, J., Meehl, G. A., Moss, R., Riahi, K., & Sanderson, B. M. (2016). The Scenario Model Intercomparison Project (ScenarioMIP) for CMIP6. *Geoscientific Model Development*, *9*(9), 3461–3482. https://doi.org/10.5194/gmd-9-3461-2016

Pausata, F. S. R., Chafik, L., Caballero, R., & Battisti, D. S. (2015). Impacts of high-latitude volcanic eruptions on ENSO and AMOC. *Proceedings of the National Academy of Sciences*, *112*(45), 13784–13788. https://doi.org/10.1073/pnas.1509153112

Santer, B. D., Bonfils, C., Painter, J. F., Zelinka, M. D., Mears, C., Solomon, S., Schmidt, G. A., Fyfe, J. C., Cole, J. N. S., Nazarenko, L., Taylor, K. E., & Wentz, F. J. (2014). Volcanic contribution to decadal changes in tropospheric temperature. *Nature Geoscience*, *7*(3), 185–189. https://doi.org/10.1038/ngeo2098

Schmidt, A., Mills, M. J., Ghan, S., Gregory, J. M., Allan, R. P., Andrews, T., Bardeen, C. G., Conley, A., Forster, P. M., Gettelman, A., Portmann, R. W., Solomon, S., & Toon, O. B. (2018). Volcanic Radiative Forcing From 1979 to 2015. *Journal of Geophysical Research: Atmospheres*, *123*(22), 12491–12508. https://doi.org/10.1029/2018JD028776

Mulcahy, J. P., Jones, C. G., Rumbold, S. T., Kuhlbrodt, T., Dittus, A. J., Blockley, E. W., Yool, A., Walton, J., Hardacre, C., Andrews, T., Bodas-Salcedo, A., Stringer, M., de Mora, L., Harris, P., Hill, R., Kelley, D., Robertson, E., & Tang, Y. (2023). UKESM1.1: Development and evaluation of an updated configuration of the UK Earth System Model. *Geoscientific Model Development Discussions*, in press. https://doi.org/10.5194/gmd-2022-113

Sigl, M., Toohey, M., McConnell, J. R., Cole-Dai, J., & Severi, M. (2022). Volcanic stratospheric sulfur injections and aerosol optical depth during the Holocene (past 11 500 years) from a bipolar ice-core array. *Earth System Science Data*, *14*(7), 3167–3196. https://doi.org/10.5194/essd-14-3167-2022

Sigl, M., Winstrup, M., McConnell, J. R., Welten, K. C., Plunkett, G., Ludlow, F., Büntgen, U., Caffee, M., Chellman, N., Dahl-Jensen, D., Fischer, H., Kipfstuhl, S., Kostick, C., Maselli, O. J., Mekhaldi, F., Mulvaney, R., Muscheler, R., Pasteris, D. R., Pilcher, J. R., … Woodruff, T. E. (2015). Timing and climate forcing of volcanic eruptions for the past 2,500 years. *Nature*, *523*(7562), 543–549. https://doi.org/10.1038/nature14565

Stoffel, M., Khodri, M., Corona, C., Guillet, S., Poulain, V., Bekki, S., Guiot, J., Luckman, B. H., Oppenheimer, C., Lebas, N., Beniston, M., & Masson-Delmotte, V. (2015). Estimates of volcanic-induced cooling in the Northern Hemisphere over the past 1,500 years. *Nature Geoscience*, *8*(10). https://doi.org/10.1038/ngeo2526

Timmreck, C., Mann, G. W., Aquila, V., Hommel, R., Lee, L. A., Schmidt, A., Brühl, C., Carn, S., Chin, M., Dhomse, S. S., Diehl, T., English, J. M., Mills, M. J., Neely, R., Sheng, J., Toohey, M., & Weisenstein, D. (2018). The Interactive Stratospheric Aerosol Model Intercomparison Project (ISA-MIP): Motivation and experimental design. *Geoscientific Model Development*, *11*(7), 2581–2608. https://doi.org/10.5194/gmd-11-2581-2018

Zambri, B., Robock, A., Mills, M. J., & Schmidt, A. (2019). Modeling the 1783–1784 Laki Eruption in Iceland: 2. Climate Impacts. *Journal of Geophysical Research: Atmospheres*, *124*(13), 6770–6790. https://doi.org/10.1029/2018JD029554

AGU PUBLICATIONS

Geophysical Research Letters

Supporting Information for

Climate Projections Very Likely Underestimate Future Volcanic Forcing and its Climatic Effects

Man Mei Chim[1], Thomas J. Aubry[2], Nathan Luke Abraham[1,3], Lauren Marshall[4], Jane Mulcahy[5], Jeremy Walton[5], Anja Schmidt[1,6,7]

[1]Centre for Atmospheric Science, Yusuf Hamied Department of Chemistry, University of Cambridge, Cambridge, United Kingdom
[2]Department of Earth and Environmental Sciences, University of Exeter, Penryn, United Kingdom
[3]National Centre for Atmospheric Science, United Kingdom
[4]Department of Earth Sciences, Durham University, Durham, United Kingdom
[5]Met Office, FitzRoy Road, Exeter, EX1 3PB, UK
[6]German Aerospace Center (DLR), Institute of Atmospheric Physics (IPA), Oberpfaffenhofen, Germany
[7]Ludwig-Maximilians University Munich, Meteorological Institute, Munich, Germany

Contents of this file

Text S1 to S3
Figures S1 to S6
Tables S1 to S4

Additional Supporting Information (Files uploaded separately)

Table S1. Time-averaged volcanic effects relative to the magnitude of anthropogenic contribution on large-scale climate indicators over the period of 2015 to 2100. Data for Figure 5 in the main text.

Table S2. Year range of crossing 1.5 °C, 2 °C, and 3 °C for all the model scenarios. The numbers in the bracket refer to the uncertainty range of the maximum and minimum ensemble members.

Table S3. List of volcanoes used in deriving the mass eruption rate for large-magnitude eruptions. The latitudes, longitudes and vent altitudes are obtained from the Smithsonian Global Volcanism Program (Global Volcanism Program, 2022).

Table S4. Values of input parameters related to magma properties in Plumeria.

Introduction

The supplementary information includes details of the resampling of eruption source parameters (Text S1), description of the UKESM-VPLUME framework (Text S2), and the procedures to remove the anthropogenic signal from time series data (Text S3). Data files including the large-magnitude and small-magnitude eruption datasets used in resampling (d01.xslx) and the future eruption scenarios used in model simulation (d02.xslx) are uploaded as additional information.

Text S1. Resampling of eruption source parameters.

In this study, we resample eruption source parameters, including SO_2 mass, eruption location, and mass eruption rate, from the ice-core and satellite-based volcanic SO_2 emission datasets (Sigl et al., 2022; Carn, 2022) and the Smithsonian Global Volcanism Program (Global Volcanism Program, 2022). The following sections provide more details on the resampling of the eruption source parameters.

i. SO_2 mass

We use 3 Tg of SO_2 as the threshold to define "small-magnitude" and "large-magnitude" eruptions and resample small-magnitude eruptions only from the satellite record. Large-magnitude eruptions are resampled from the combined bipolar ice-core array and satellite records. For both datasets, the probability of any specific eruption to occur on a given day is the inverse of the number of days in the dataset, i.e., 2.4×10^{-7} and 6.6×10^{-5} for the large- and small-magnitude eruption input datasets, respectively. To generate stochastic eruption scenarios for 2015-2100, we perform Monte Carlo simulations by generating random numbers between 0 and 1 from a uniform distribution for each day of the 2015-2100 period and each eruption in the input datasets. An eruption in one of the input datasets is triggered if the random number drawn is lower than the probability of that eruption to occur (i.e., 2.4×10^{-7} or 6.6×10^{-5}). We first generate 1000 future large- and small-magnitude eruption scenarios separately and combine both eruption chronologies to obtain 1000 unique future eruption scenarios from 2015 to 2100.

In addition to the details described in the main text, we have the following assumptions:

(1) In the satellite record, we assume that explosive eruptions that occur in the same eruption phase (i.e., with the next eruption occurring within 7 days) are one single eruption event. The SO_2 mass from these combined eruptions is summed and the eruptive plume height is the average plume height weighted by the SO_2 mass of the events.

(2) We assume that sulfate aerosol deposition from all explosive eruptions recorded in Holvol corresponds to stratospheric emissions. We note that a recent study on the isotopic signature of ice-core sulfate from Antarctic ice cores showed that several previously attributed Southern Hemisphere eruption events in the ice-cores record in Sigl et al. (2015) in fact originated from the troposphere (Gautier et al., 2019). Since this sulfate isotopic study is limited to the record in Sigl et al. (2015), we decide to assume that all explosive volcanic SO_2 emissions in Holvol are stratospheric emissions.

ii. Eruption location and vent altitude

The majority of volcanic eruptions with volcanic sulfate deposits recorded in ice core records are from unknown sources (represented as triangles in Figure S1). The sulfate signals from the synchronized bipolar ice cores determine the eruption hemisphere of these unknown eruption events, i.e., attributed as extra-tropical Northern Hemisphere event for Arctic-only sulfate signal, Tropical event for bipolar sulfate signals, and extra-tropical Southern Hemisphere event for Antarctic-only sulfate signal. We only know the exact eruption latitudes and longitudes for eruptions recorded by satellite measurements and those with known sources in the bipolar ice-core record. To obtain a realistic distribution of eruption location in the stochastic future eruption scenarios, we randomly resample the eruption location and vent altitude for volcanoes among those that had confirmed explosive eruptions with volcanic explosivity index (VEI) > 3 in the Holocene from the Smithsonian Global Volcanism Program Holocene Eruption database (Global Volcanism Program, 2022) and with a latitude belonging to the latitudinal band of the eruption resampled. We choose latitudinal boundaries at 30 °N/S to distinguish the eruption hemispheres, which correspond to the edges of the tropical pipes (Butchart et al., 2014). This allows the eruption location distribution in the stochastic scenarios to resemble that in the Holocene record and the eruptions to occur at real locations of volcanoes instead of hypothetical latitudes and longitudes.

ii. Mass eruption rate

Like SO_2 mass, the mass eruption rate is resampled. However, this parameter is absent from the ice-core and satellite datasets, so we need to attribute a mass eruption rate for each eruption in these records. The mass eruption rate for each eruption from the satellite record is inverted using Plumeria (see UKESM-VPLUME section) from the satellite-measured eruptive plume height, vent altitude, and the atmospheric profile from the ERA5 reanalysis dataset (Hersbach et al., 2019) at the eruption date and location. We assume that eruptions recorded in ice-core have an SO_2 injection height of 23 km above sea level, consistent with that observed for the 1991 Mt. Pinatubo eruption (Guo et al., 2004; Fero et al., 2009). We then invert the mass eruption rate from this plume height using Plumeria. We perform this inversion for 9 locations corresponding to 9 known eruptions in the ice-core dataset, with three locations each in the extra-tropical Northern Hemisphere, the Tropics, and the extra-tropical Southern Hemisphere (Table S3). We obtain decadal-averaged atmospheric profiles at each eruption location from the UKESM pre-industrial control run. The average of the 9 mass eruption rates obtained using this procedure is 6.6×10^8 kg/s, and we use this value for all eruptions in the ice-core record.

The resampling datasets for large- and small-magnitude eruptions and the final input eruption scenarios for all VOLC runs (i.e., VOLC2.5, VOLC50-1, VOLC50-2, and VOLC98) with eruption source parameters are available in separate data files in the Supplementary Information.

Text S2. UKESM-VPLUME framework.

UKESM-VPLUME is a plume-aerosol-chemistry-climate modeling framework that couples the 1-D eruptive plume model Plumeria (Mastin, 2007, 2014) with version 1.1 of UK Earth System Model (UKESM1.1; Mulcahy et al., 2023).

UKESM is a state-of-the-art Earth System Model based on the Hadley Centre Global Environment Model version 3 (HadGEM3), a physical global atmosphere ocean climate modelling system, and is coupled with the ocean component model, Nucleus for European

Modelling of the Ocean (NEMO), and atmospheric chemistry component model UK Chemistry and Aerosols (UKCA; Dhomse et al., 2014; Archibald et al., 2020). The UKCA atmospheric chemistry model accounts for the full atmospheric chemistry processes of volcanic sulfate aerosols, volcanic halogen species, and the evolution of aerosol particles with an interactive stratospheric aerosol module, which enables the simulation of the volcanic sulfate aerosol life cycle and radiative effects. The HadGEM3 model coupled with NEMO can simulate long-term atmospheric and ocean dynamical changes in response to climate variations.

Plumeria is a one-dimensional volcanic plume model integrating the conservation equations for mass, momentum, and energy upward through a cylindrical plume (Mastin 2007, 2014). The main model outputs are the maximum plume height defined as the height where the ascent velocity of the plume reaches zero, and the neutral buoyancy height which is defined as the height at which the density of the plume equals the ambient density. The main model inputs are (i) the eruption source conditions including the temperature, gas content, specific heat and density of the magma, vent diameter, vent altitude, and the initial exit velocity; and (ii) the atmospheric condition at the eruption location, i.e., the vertical profile of the temperature, pressure levels, wind speed, wind direction, and relative humidity.

The mass eruption rate (M_0) of the eruption is a key input in Plumeria, which is calculated from the eruption source parameters:

$$M_0 = \pi \rho_0 R_0^2 U_0$$

where ρ_0 is the density of the ash-gas jet (in kg/m^3), which is dependent on the temperature and gas content of the magma, R_0 is the vent radius (in m), and U_0 is the exit velocity of the jet (in m/s).

We assume that the eruption source parameters related to magma properties are the same across all eruptions in our future eruption scenarios (see Table S4 for the values used in this study). We fix the ratio of the vent radius to the square of exit velocity at 0.02 to ensure that the eruptive plume is a buoyant plume in the model. This ratio is proportional to the Richardson number, which is a parameter governing the stability of the eruptive column (e.g., Aubry and Jellinek, 2018).

Last, the main model parameters are the radial (α) and wind (β) entrainment coefficients which govern the rate of turbulent entrainment of atmosphere into the rising volcanic plume. We use values of $\alpha = 0.1$ and $\beta = 0.25$ which result in the best agreement between a similar one-dimensional plume model and a dataset of well-observed eruptions (Aubry and Jellinek, 2018).

In the UKESM-VPLUME framework, we couple Plumeria with version 11.7 of the UKCA atmospheric chemistry model in UKESM version 1.1 to calculate the eruptive plume height during eruption at every model timestep. The SO_2 injection lasts for 24 hours for each eruption. During the eruption and at every timestep of the atmospheric model used in UKESM (i.e., every 20 minutes), the vertical profiles of atmospheric conditions simulated by UKESM are passed interactively to Plumeria. Plumeria then calculates the eruptive plume height with the prescribed eruption source parameters and the instantaneous atmospheric conditions. The calculated plume height is then passed to the UKCA model to inject volcanic SO_2 mass at the eruption location. In this study, the volcanic SO_2 for all eruptions is assumed to be injected at the neutral buoyancy level in the calculation of mass eruption rate and the UKESM-VPLUME framework (injected using a Gaussian profile). The eruptive plume heights of eruptions are thus consistent with the climate conditions simulated by UKESM (Figure S6), which allows us to account for the impacts of global warming on eruptive plume height.

Text S3. Removal of anthropogenic trend in time series data

In this study, we remove the anthropogenic signal in the time series data of all VOLC runs in order to compare the annual mean or decadal mean volcanic impacts on large-scale climate indicators (see probability density functions in Figure 3 and 4). For each large-scale climate indicators, we first calculate the anthropogenic signal from 2015 to 2100 by fitting a third-order polynomial function to the annual mean ensemble mean of the NOVOLC run. We then subtract the anthropogenic signal from all the annual mean time series in VOLC and NOVOLC runs to obtain detrended annual mean time series data (as in Figure 3b). In the calculation of detrended decadal mean time series, we subtract the annual mean anthropogenic signal from each ensemble member of the VOLC and NOVOLC runs before calculating the decadal mean. We then plot the detrended decadal mean for all the ensemble members as one probability density function (as in Figure 4).

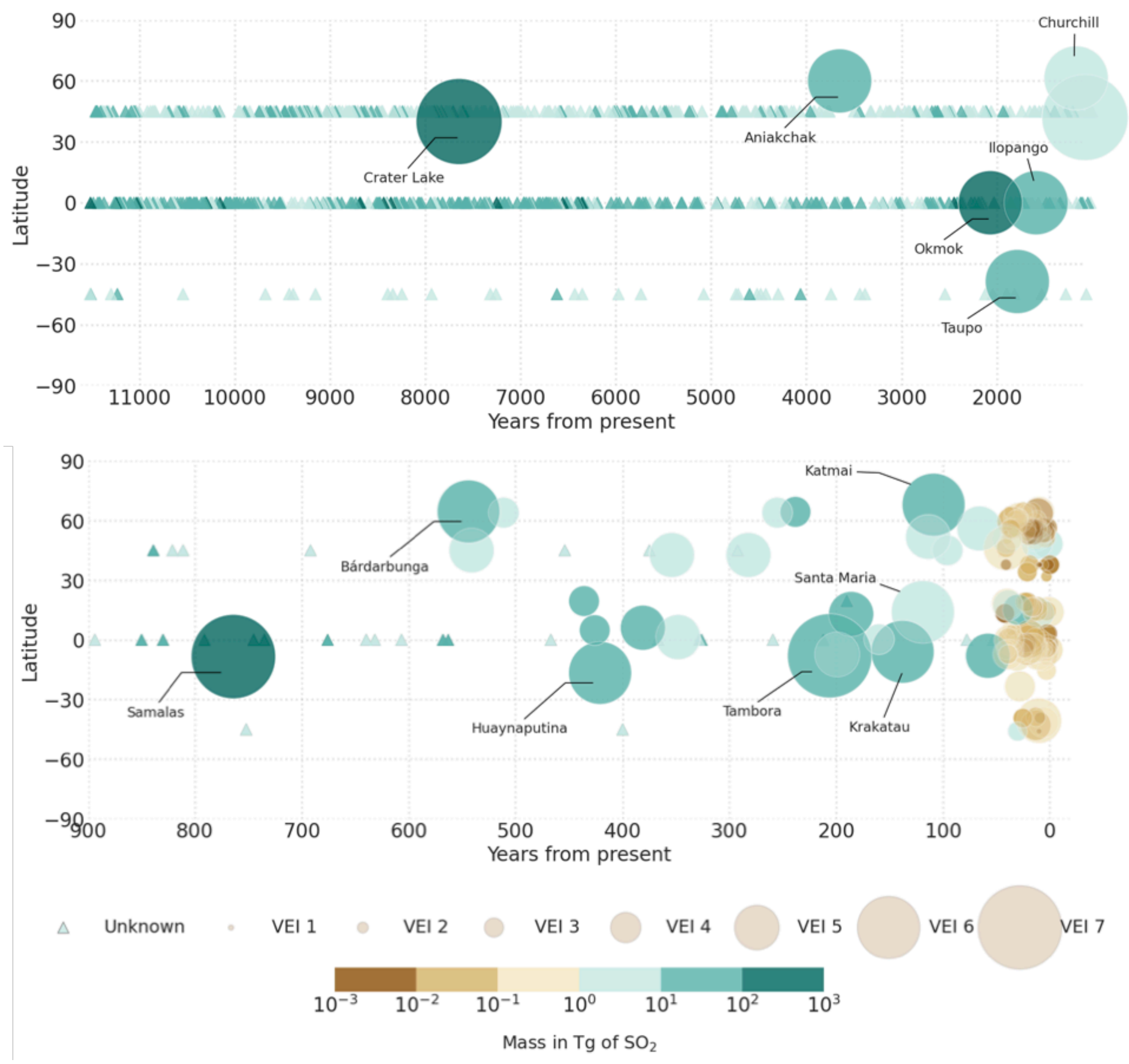

Figure S1. Historical explosive eruptions from ice core and satellite records in the past 11,500 years from Holvol ice-core dataset and satellite datasets after data filtering. Unknown eruptions with hemispheric information only are assigned with fixed latitudes (i.e., at 0° and 45°N/S). The Volcanic Explosivity Index (VEI) of the eruptions is obtained from the Smithsonian Global Volcanism Program database (Global Volcanism Program, 2022).

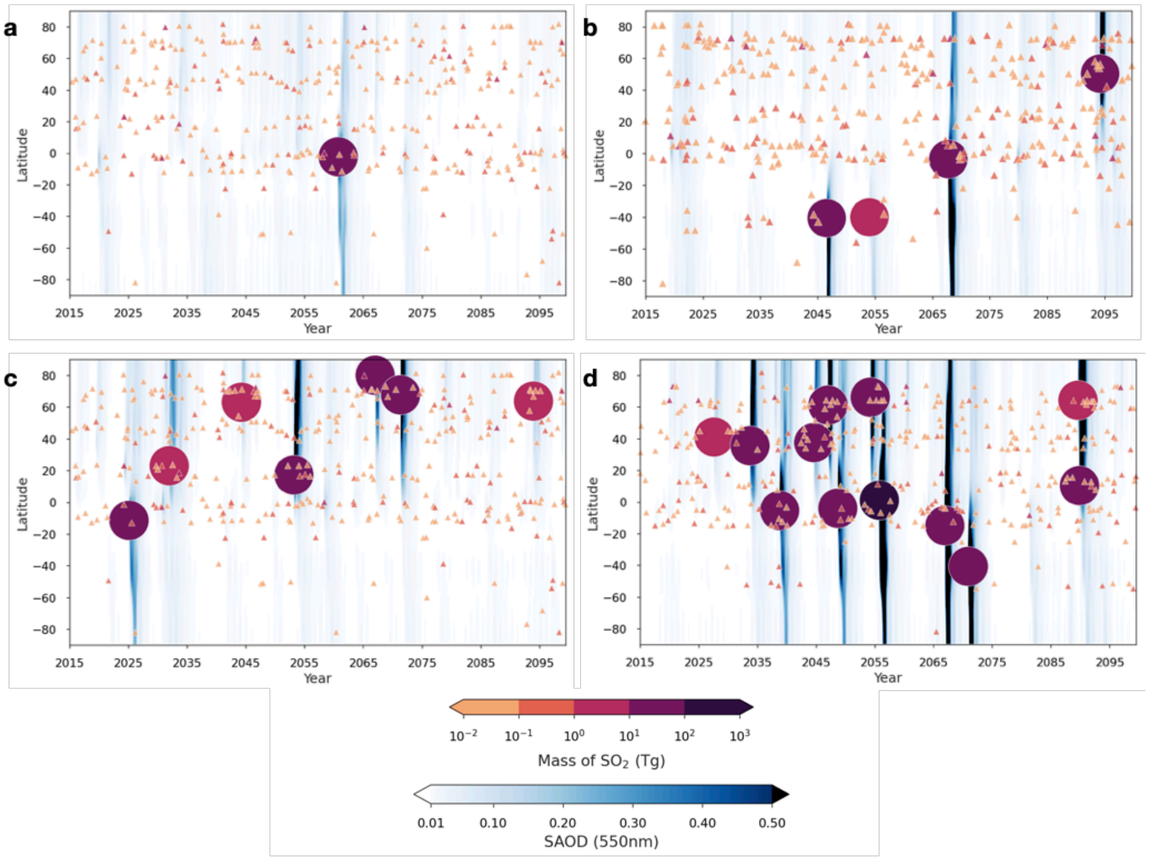

Figure S2. Zonal mean stratospheric aerosol optical depth (SAOD) in 550 nm (blue shading) and eruption time series (markers) with mass of SO_2 from 2015 to 2100 for (a) VOLC2.5, (b) VOLC50-1, (c) VOLC50-2, (d) VOLC98. Large-magnitude (> 3 Tg of SO_2) and small-magnitude (< 3 Tg of SO_2) eruptions are represented in circles and triangles respectively.

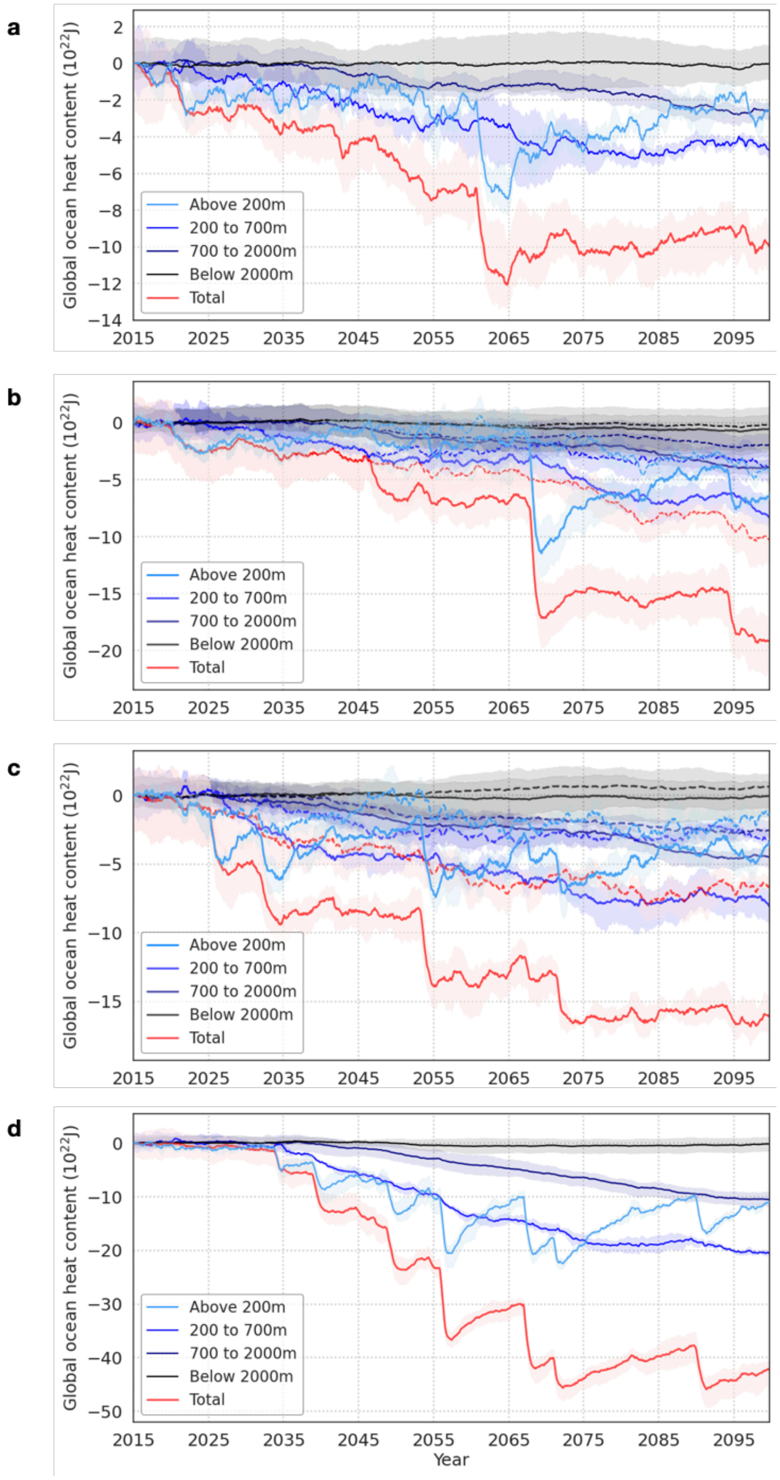

Figure S3. Global monthly-mean ocean heat content anomaly relative to NOVOLC for (a) VOLC2.5, (b) VOLC50-1 (solid lines) and VOLC50-1S (dotted lines), (c) VOLC50-2 (solid lines) and VOLC50-2S (dotted lines), and (d) VOLC98.

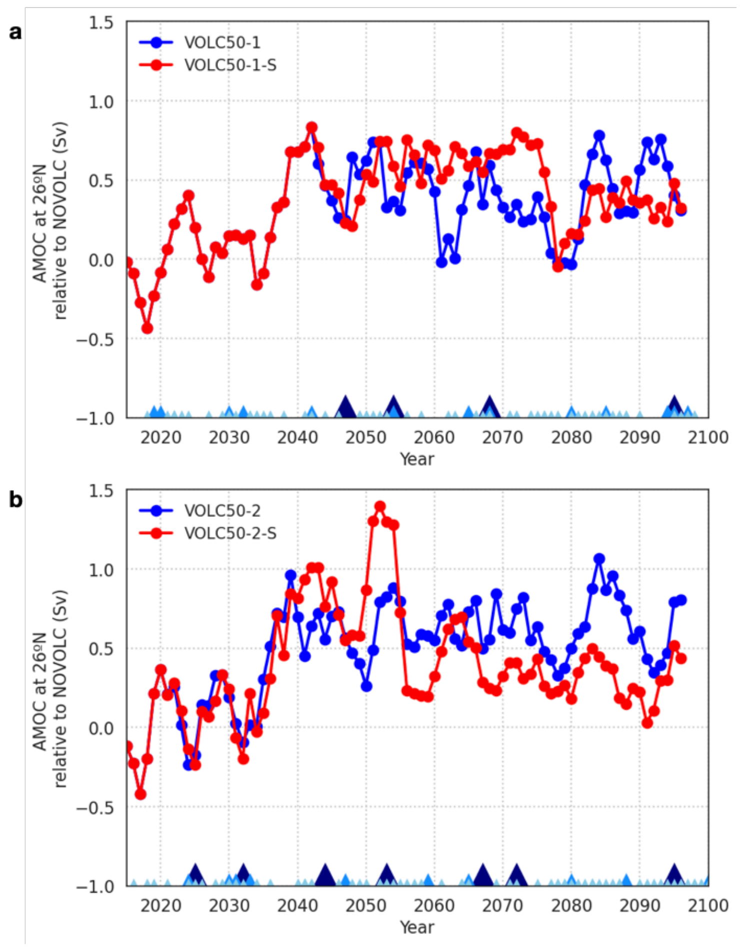

Figure S4. 5-year moving mean of Atlantic meridional overturning circulation (AMOC) at 26ºN relative to NOVOLC for (a) VOLC50-1 and VOLC50-1S, and (b) VOLC50-2 and VOLC50-2S. The triangles represent the eruptions with > 3 Tg of SO_2 (dark blue), between 1 to 3 Tg of SO_2 (blue) and < 1 Tg of SO_2 (light blue) of the scenarios.

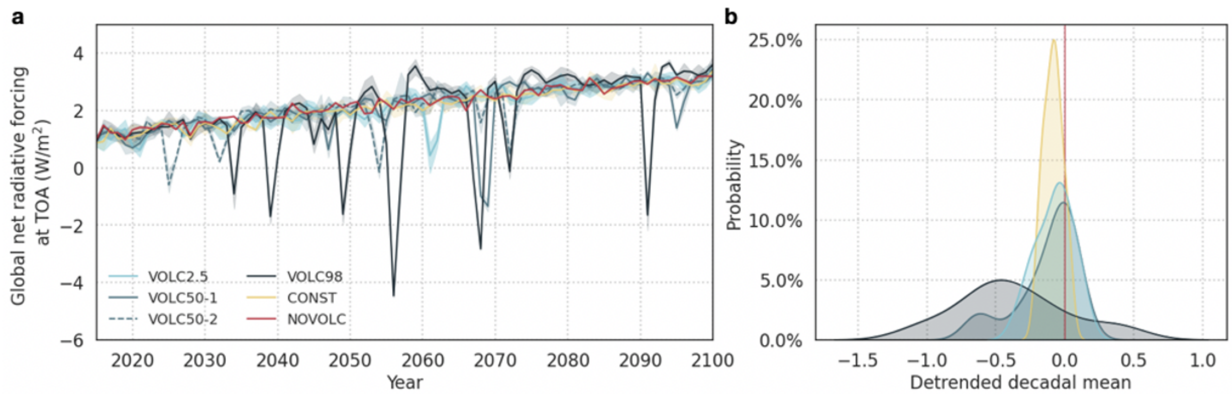

Figure S5. (a) Global annual-mean net radiative forcing at the top-of-the-atmosphere (TOA) (in W/m^2) from 2015 to 2100, and (b) the respective probability density function of the detrended decadal mean.

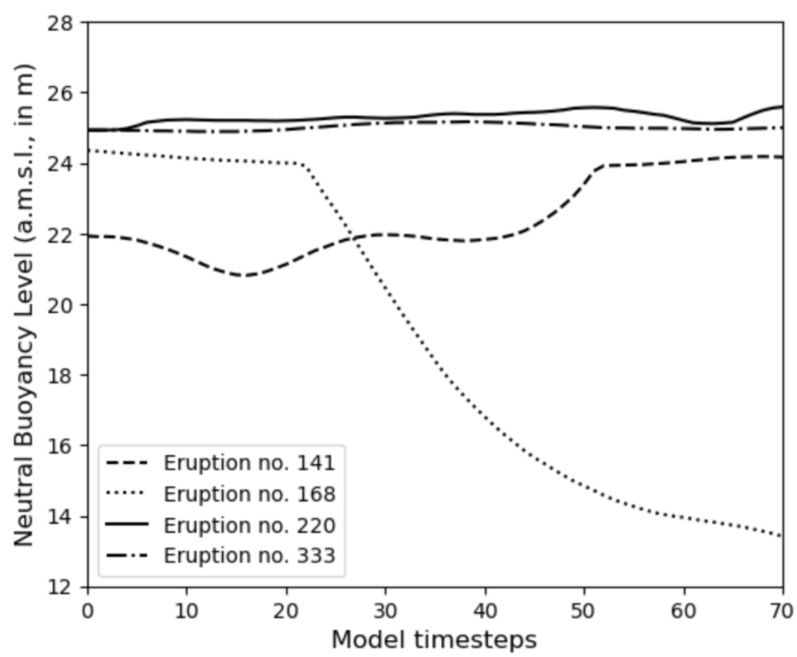

Figure S6. The time series of plume height in neutral buoyancy level above mean sea level (in m) for four large-magnitude eruptions during SO_2 mass injection in the UKESM-VPLUME framework. The data is extracted from one of the ensemble members for the VOLC50-1 run.

Climate indicators	VOLC50-1	VOLC50-1S	VOLC50-2	VOLC50-2S	CONST	VOLC-98	VOLC-2.5
Global mean surface air temperature (°C)	-0.20 (-4.0%)	-0.11 (-2.1%)	-0.24 (-4.8%)	-0.09 (-1.8%)	-0.12 (-2.4%)	-0.56 (-11.1%)	-0.16 (-3.1%)
Global ocean heat content ($\times 10^{22}$ J)	-8.34 (-3.1%)	-4.63 (-1.7%)	-10.70 (-3.9%)	-4.63 (-1.7%)	-6.52 (-2.4%)	-24.20 (-8.9%)	-6.64 (-2.4%)
Global thermosteric sea level rise (m)	-0.012 (-3.3%)	-0.006 (-1.8%)	-0.015 (-4.2%)	-0.007 (-1.9%)	-0.009 (-2.5%)	-0.033 (-9.6%)	-0.009 (-2.6%)
Global precipitation flux (mm/day)	-0.018 (-6.3%)	-0.009 (-3.3%)	-0.020 (-7.1%)	-0.008 (-2.7%)	-0.010 (-3.6%)	-0.052 (-18.2%)	-0.014 (-4.8%)
Global net radiative forcing at top-of-the-atmosphere (W/m^2)	-0.15 (-6.8%)	-0.08 (-3.6%)	-0.13 (-5.7%)	-0.05 (-2.4%)	-0.08 (-3.8%)	-0.34 (-15.0%)	-0.08 (-3.5%)
Atlantic Meridional Overturning Circulation at 26°N (Sv)	+0.31 (+5.5%)	+0.36 (+6.5%)	+0.49 (+8.7%)	+0.38 (+6.7%)	+0.28 (+4.9%)	+0.93 (+16.6%)	+0.26 (+4.6%)
Global sea ice extent (million km^2)	+0.52 (+3.4%)	+0.21 (+1.4%)	+0.68 (+4.4%)	+0.22 (+1.4%)	+0.20 (+1.3%)	+1.53 (+9.9%)	+0.43 (+2.8%)
Arctic sea ice extent (million km^2)	+0.31 (+3.4%)	+0.17 (+1.9%)	+0.48 (+5.4%)	+0.16 (+1.8%)	+0.16 (+1.7%)	+0.81 (+9.1%)	+0.18 (+2.1%)
Antarctic sea ice extent (million km^2)	+0.22 (+3.3%)	+0.04 (+0.6%)	+0.20 (+3.0%)	+0.06 (+0.9%)	+0.04 (+0.6%)	+0.72 (+11.1%)	+0.25 (+3.9%)

Table S1. Time-averaged volcanic effects relative to the magnitude of anthropogenic contribution on large-scale climate indicators over the period of 2015 to 2100. Data for Figure 5 in the main text.

Model scenarios	Year of crossing		
	1.5 ^{o}C	2 ^{o}C	3 ^{o}C
NOVOLC	2019.40 (2018.87 - 2019.75)	2029.00 (2028.03 - 2029.75)	2047.77 (2046.40 - 2048.57)
CONST	2020.76 (2019.77 - 2021.40)	2031.06 (2029.79 - 2032.20)	2049.38 (2047.96 - 2050.73)
VOLC2.5	2021.20 (2021.09 - 2021.27)	2031.45 (2031.22 - 2031.78)	2050.53 (2049.73 - 2051.14)
VOLC50-1	2021.04 (2020.02 - 2022.60)	2031.13 (2029.99 - 2033.15)	2049.01 (2047.87 - 2051.17)
VOLC50-2	2022.59 (2022.10 - 2023.21)	2033.29 (2032.30 - 2034.09)	2051.89 (2050.45 - 2053.06)
VOLC98	2021.69 (2021.27 - 2022.67)	2036.19 (2034.17 - 2038.25)	2062.13 (2061.16 - 2063.37)

Table S2. Year range of crossing 1.5 ^{o}C, 2 ^{o}C, and 3 ^{o}C for all the model scenarios. The numbers in the bracket refer to the uncertainty range of the maximum and minimum ensemble members.

Volcano	Latitude	Longitude	Vent altitude (m)
Mount Churchill	61.25	-141.750	5005
Mount Katmai	58.75	-154.963	2047
Changbaishan	42.50	128.080	2744
El Chichón	17.50	93.230	1205
Mount Pinatubo	15.00	120.350	1486
Mount Tambora	-8.75	118.000	2850
Taupō	-38.75	176.000	760
Calbuco	-41.25	-72.618	1974
Mount Hudson	-46.25	-72.970	1905

Table S3. List of volcanoes used in deriving the mass eruption rate for large-magnitude eruptions. The latitudes, longitudes and vent altitudes are obtained from the Smithsonian Global Volcanism Program database (Global Volcanism Program, 2022).

Input parameters	Values used
Magma temperature	1100 ^{o}C
Mass fraction of gas in magma	5 wt.%
Specific heat of magma	1280 J/kg K
Magma density	2350 kg/m^3

Table S4. Values of input parameters related to magma properties in Plumeria.

Data Set S1. The input datasets for large-magnitude (> 3 Tg of SO_2) and small-magnitude (< 3 Tg of SO_2) historical eruptions from the ice-core and satellite datasets used for resampling.

Data Set S2. The eruption time series and information of the future stochastic scenarios VOLC2.5, VOLC50-1, VOLC50-2 and VOLC98.